Back to Session Subjects

LOCATION AND QUANTIFICATION OF HELICOPTER NOISE SOURCES IN A WIND TUNNEL

Stefan Oerlemans

National Aerospace Laboratory, NLR
Voorsterweg 31, 8316 PR Marknesse The Netherlands
e-mail: stefan@nlr.nl

Key words: helicopter noise, acoustic testing, phased arrays

Abstract: In the framework of the European HeliNOVI project an acoustic wind tunnel study was conducted into helicopter tail rotor noise. The goal of these tests in the DNW-LLF was to investigate (1) the relative importance of main rotor (MR) and tail rotor (TR) noise for different flight conditions, (2) MR-TR interaction noise, and (3) tail rotor noise reduction concepts. Besides the conventional measurement techniques, such as an inflow microphone traverse, blade pressure transducers and PIV (Particle Image Velocimetry), an out-of-flow phased microphone array was applied to locate and quantify the different helicopter noise sources. In the present paper the array results are analyzed, and the capabilities and limitations of the array technique for helicopters are discussed. The array analysis showed that TR noise is most important for climb and high-speed level flight. By comparing TR noise spectra for the 'TR only' and 'MR+TR' cases, small interaction effects could be shown. Furthermore, several TR noise reduction concepts were assessed, which showed that, besides a reduction of rotor tip speed, reversal of TR sense of rotation is most efficient. Using a processing method for rotating sources, small noise differences between individual MR blades could be identified. Surprisingly, this method also clearly showed the dependence of TR noise on MR azimuth for the cases where TR noise is dominant. The array results were also compared to the more conventional inflow footprints, which showed that the array provides additional information on source locations and directivity. With regard to noise reduction concepts, source ranking, and interaction effects, the array results are generally consistent with the inflow footprints.

1 INTRODUCTION

In the framework of the European HeliNOVI project[1,2], an acoustic wind tunnel study was conducted into helicopter rotor noise. The goal of these tests in the DNW-LLF was to investigate (1) the relative importance of main rotor (MR) and tail rotor (TR) noise for different flight conditions, (2) MR-TR interaction noise, and (3) tail rotor noise reduction concepts. Besides the conventional measurement techniques, such as an inflow microphone traverse, blade pressure transducers and PIV (Particle Image Velocimetry), an out-of-flow phased microphone array was applied to locate and quantify the different helicopter rotor noise sources. This paper describes the phased array measurements and their results.

Although the phased array technique has been applied previously in many aeroacoustic studies (e.g. airframe noise[3,4], wind turbine noise[5,6], and noise from airfoil sections[7]), its application to helicopter rotor noise has been rather limited[8,9,10]. Therefore, besides a systematic analysis of the array results for different test conditions and rotor configurations, the present paper will also discuss the capabilities and limitations of this technique for helicopter rotor noise. The array results will be compared to the inflow footprints to check the consistency between the two different methods. The present paper focuses on the description and interpretation of the experimental results, rather than examining the source mechanisms in detail. A limited analysis of the results has already been presented in Ref. 2.

The structure of this paper is as follows: first, the experimental method is described in Section 2. Next, the test results are presented and discussed in Section 3. Finally, the conclusions are summarized in Section 4.

2 EXPERIMENTAL METHOD

This section gives an overview of the experimental method. Section 2.1 describes the test set-up, followed by the data acquisition and processing techniques in Section 2.2. The test program is given in Section 2.3.

2.1 Test set-up

The test campaign was performed in the 8x6 m^2 open jet test section of the DNW-LLF wind tunnel (Fig. 1). The 40% BO-105 helicopter model consisted of dynamically and Mach scaled main rotor blades, a geometrically scaled fuselage, and a teetering Mach scaled tail rotor system. The 4-bladed main rotor had a radius of 2 m and rotated in anti-clockwise direction (seen from above) at a nominal RPM of 1043. Two different (2-bladed) tail rotors were used, with NACA0012 and S102 airfoils. Both had a radius of 0.38 m and rotated at a nominal RPM of 5215 (i.e. 5 times the RPM of the main rotor). The normal TR sense of rotation was "advancing side down", but the NACA0012 tail rotor could also run in the "advancing side up" mode. The main rotor, tail rotors, and fuselage were instrumented with in total 118 dynamic pressure sensors. More details about the model and instrumentation can be found in Ref. 2.

Fig. 1: Test set-up in DNW-LLF, with the out-of-flow microphone array in red

Acoustic measurements were done both inside and outside the wind tunnel flow. The inflow measurements were done using 16 ½-inch microphones mounted on a U-shaped wing support (Fig. 1). The microphones were aligned with the tunnel axis and were pointing upstream. The wing support was lined with foam to suppress reflections, and could be traversed in streamwise direction in steps of 0.5 m. The vertical distance between the main rotor hub and the horizontal part of the wing support was in most cases 2.3 m.

The out-of-flow phased array consisted of 140 ½-inch microphones in an open metal grid of 4x4 m^2, and was fixed to the inflow microphone traverse (Fig. 1). The streamwise distance between the array center and the inflow traverse was 2.7 m. The array microphones were equipped with wind screens to prevent flow-induced noise. The vertical distance between the microphones and the center of the main rotor was 7.15 m (descent and level flight) or 6.85 m (climb), and the lateral distance between the array center and the tunnel centerline was 0.5 m (to the side of the TR).

The streamwise array position was specified with respect to the position of the main rotor (X_{MR}=0 by definition). Note that the axial position of the main rotor in the wind tunnel was not the same for all flight conditions. The array was traversed in streamwise direction, and array measurements were generally done for an upstream position (X_{array}=-2.7 m) and for a position below the model (X_{array}=1.5 m). For the climb condition, the second measurement position was at X_{array}=0.8 m due to geometrical constraints. Fig. 2 shows the microphone locations for the position below the model (X_{array}=1.5 m).

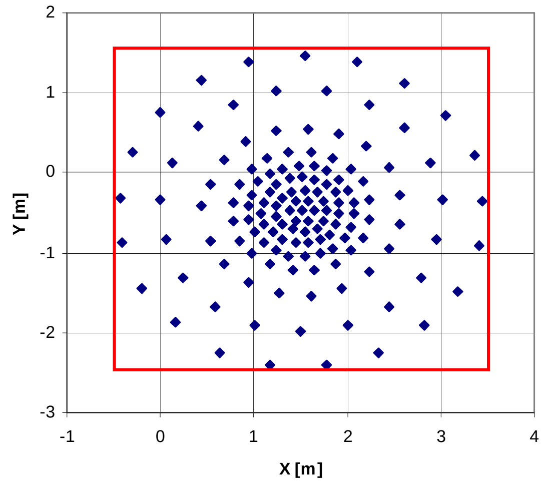

Fig. 2: Lay-out of microphone array

2.2 Data acquisition and processing

All acoustic data were acquired using the DNW/NLR multi-channel data-acquisition system[11]. For the inflow microphones, measurements were done in the 'step-by-step' mode with a streamwise step size of 0.5 m. Acoustic data were recorded in three different ways: phase-locked with the main rotor (2048 samples/revolution), phase-locked with the tail rotor (512 samples/revolution), and at a fixed sample rate of 51.2 kHz ("free-run" mode). A 10 Hz high-pass filter was used to suppress the DC component of the pressure signals. The inflow microphone signals were further processed to pressure-time histories, acoustic spectra, and noise footprints using time-averaged pressure histories. Full-scale dB(A) values were obtained by first converting the measured spectra to full-scale (frequencies divided by 2.5) and then applying A-weighting[2].

Acoustic data from the array microphones were synchronously measured at a fixed sample frequency of 51.2 kHz and a measurement time of 30 seconds. Trigger signals from main and tail rotor were also recorded to enable phase-locked averaging if desired. A high-pass filter (-3 dB at 500 Hz) was used to enhance the dynamic range for high frequencies. The levels in this paper are corrected for the filter characteristics. The frequency response of the individual array microphones was taken from calibration sheets. The acoustic data were processed using a block size of 4096 with a Hanning window and an overlap of 50%, yielding 750 averages and a narrowband frequency resolution of 12.5 Hz. Random averaging was applied (i.e. not synchronised to MR or TR revolutions), so that both main and tail rotor noise sources will show up in the results (if present). Synchronised averaging was also applied for some cases, to produce acoustic source plots of MR or TR noise only, but these results will not be presented here.

Conventional beamforming[12] was applied in the frequency domain to obtain acoustic source plots in 1/3-octave bands. To improve the resolution and further reduce background noise from the tunnel, the main diagonal in the cross power matrix (autopowers) was discarded. The effect of sound refraction by the tunnel shear layer was corrected using a simplified Amiet method[13]. The array scan plane was placed in the main rotor plane and was rotated in accordance with the model angle of attack. The scan levels were normalized to a distance of

0.282 m [$(4\pi)^{-1/2}$], so that for a monopole source the peak level in the source plot corresponds to the Sound Power Level. The noise sources from the main and tail rotor were quantified by applying a power integration method[3] to integration contours around the main and tail rotor (Fig. 3). In a number of cases the integrated levels were corrected for background noise and for the mutual influence between both integration areas (i.e the effect of a MR source on the integrated TR noise level and vice versa).

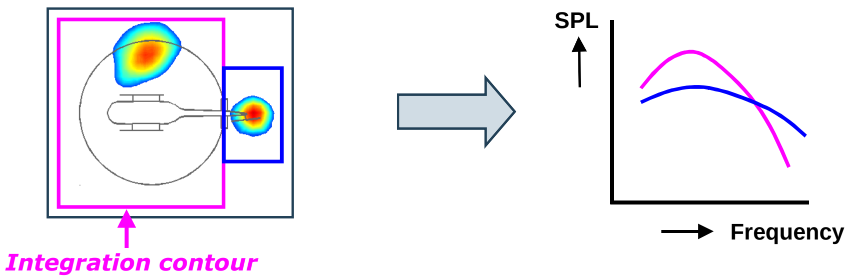

Fig. 3: Schematic representation of the power integration method

Despite the RPM ratio of about 5, the phase difference between main and tail rotor was generally random, since the driving mechanisms for both rotors were not synchronized mechanically. However, after the experiments it turned out that for some periods of time the main and tail rotor had been running in phase, i.e. the ratio of their rotational speeds was exactly 5. Since the footprints indicated that this could influence the results, the array data were checked for periods with a fixed phase difference between MR and TR (using the trigger signals). It turned out that only for one measurement such a period was present for several seconds. Comparison of the array results for this time segment with a random-phase segment showed that the results were practically the same (within 1 dB). Therefore all array measurements were processed using the full 30 seconds of measurement time.

Besides the conventional beamforming, a second processing method (ROtating Source Identifier-ROSI[9]) was applied to identify the noise sources on the individual main rotor blades. The scan plane was placed in the main rotor plane and rotated along with the main rotor blades. The start position of the blades was determined using the main rotor trigger signal. In order to limit processing time, only the first 30 revolutions after the start of each acoustic measurement were processed.

2.3 Test program

The experiments were carried out in two test campaigns, the first in July 2003 and the second in August 2004. Measurements were done done for 12° climb, 6° descent, and level flight conditions. The wind (or flight) speeds were 33 m/s for climb and descent, and 33, 44, and 60 m/s for level flight. The model was tested in 'MR only', 'TR only', and 'MR+TR' configuration. Unless explicitly mentioned otherwise, the results in this paper are for the MR+TR configuration. The following TR noise reduction concepts were tested:

- S102 TR versus NACA0012 TR
- 10% reduced tip speed (for both the main- and tail rotor)
- reversed sense of rotation (for the NACA0012 TR)
- change in TR position (for the S102 TR)

More details about reduction concepts and model conditions (e.g. thrust, flapping angles) can be found in Ref. 2.

3 RESULTS AND DISCUSSION

In this chapter the experimental results are presented and discussed. Section 3.1 provides a systematic analysis of the array results for different conditions and configurations. In Section 3.2 the array results are compared to the inflow footprints to check the consistency between the two different methods. In order to explain the difference between inflow footprints and so-called acoustic 'source plots' from the phased array, Fig. 4 shows a picture of the test set-up with the out-of-flow microphone array, the inflow scan plane, and the array scan plane. Whereas the inflow footprints show the *overall* noise radiation (from all sources) in *different* directions, the phased array identifies the *different* sources for a *fixed* observer position (i.e. the array position). Thus, both methods provide complementary information on the location and directivity of the noise sources. This relation between inflow footprints and acoustic source plots will be further elucidated in Section 3.2. Unless explicitly mentioned otherwise, the presented results are for the 'MR+TR' configuration and for the array position below the model. Since random averaging was applied (see Section 2.2), the relative importance of MR and TR noise sources can be assessed on the basis of the array results. The results are presented in 1/3-octave bands at model scale frequencies, without A-weighting.

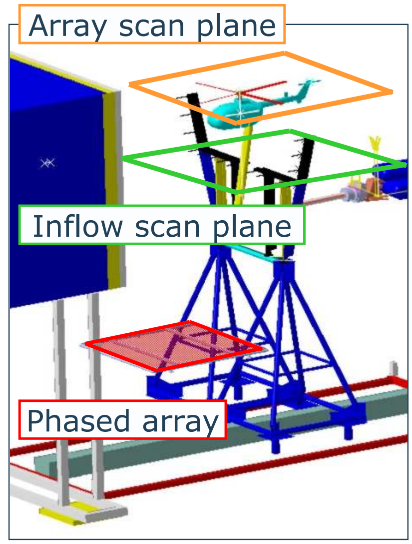

Fig. 4: Test set-up with phased array and different scan planes.

3.1 Phased array results

In this section the phased array results are discussed. First some qualitative observations in the acoustic source plots will be described. Subsequently, a quantitative analysis will be provided of the repeatability (2003 versus 2004), source ranking (MR versus TR noise), MR-TR interaction effects, and TR noise reduction concepts. Finally, the results of the ROtating Source Identifier (ROSI) are discussed.

Acoustic source plots

Fig. 5 shows example source plots, illustrating the variation in noise source location for different conditions. The range of the color scale is 12 dB for each plot. The upper row indicates that for level flight the tail rotor is dominant at low frequencies, while the main rotor is a dominant noise source at higher frequencies. The main rotor noise is produced on the advancing side. The second row shows that (at 2 kHz) the TR is dominant for climb and level flight, while the MR is dominant for the descent condition (due to Blade Vortex Interaction noise). The third row shows the source locations for the two array positions, upstream and below the model (descent flight, 2 kHz). It can be seen that for the upstream position the advancing side is dominant, while for the position below the model both sides of the rotor plane contribute to the radiated noise. Thus, by comparing the source plots for both array positions, information can be obtained on the directivity of the different noise sources.

Repeatability

The array results were quantified using a power integration method (see Section 2.2). To check the repeatability of the results, the integrated TR noise spectra from the 2003 and 2004 test campaigns were compared. Fig. 6 shows an example of this comparison for the level flight case. It can be seen that the absolute TR noise levels for the three wind speeds are typically repeatable within a few dB. The differences between the two campaigns are probably due to small changes in the model or test set-up. To avoid any doubts about the conclusions of this study, all comparisons in the remainder of this paper are made using the 2004 data.

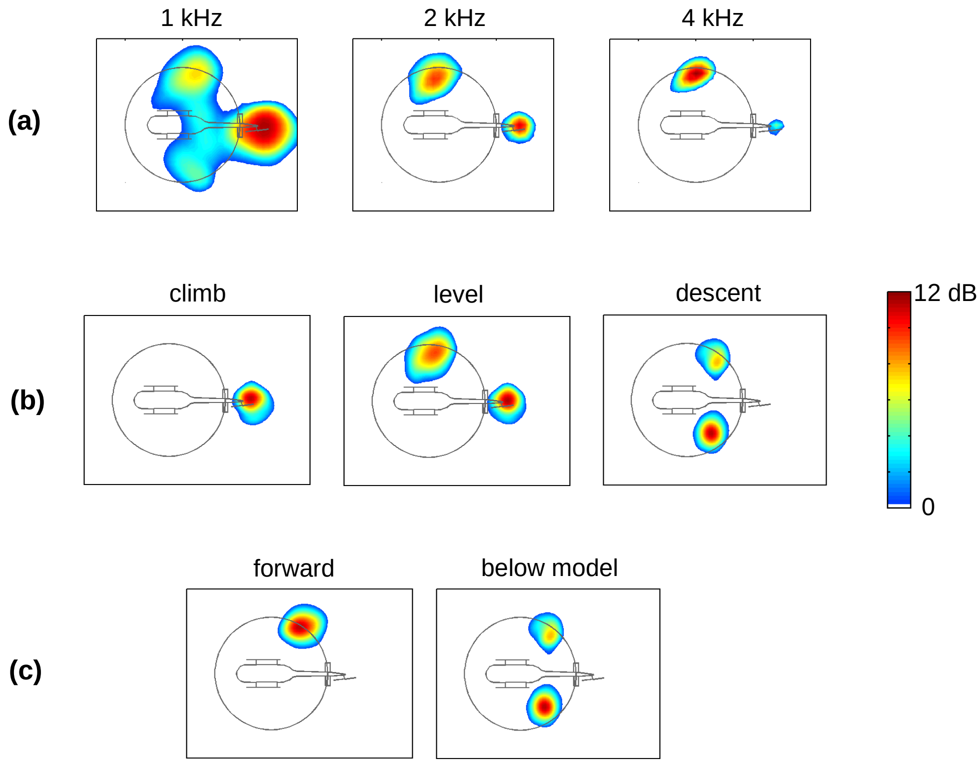

Fig. 5: Acoustic source plots illustrating the dependence of the noise source locations on (a) frequency (level flight), (b) flight condition (2 kHz), and (c) array position (descent, 2 kHz).

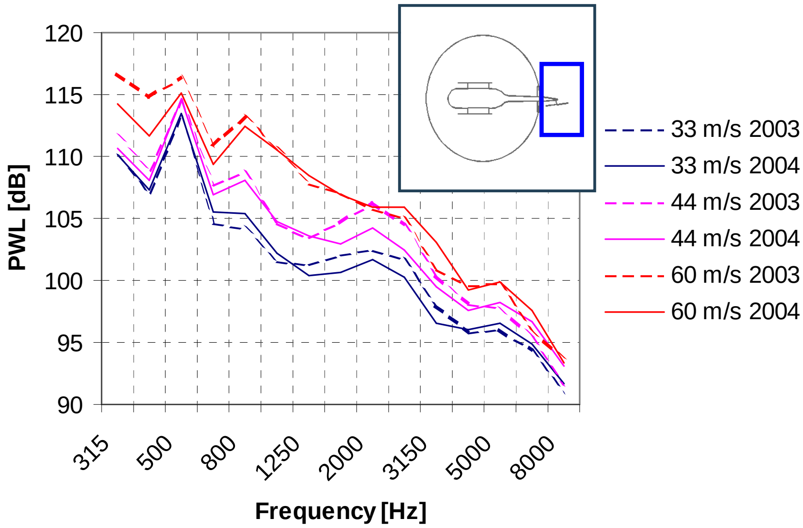

Fig. 6: Integrated TR noise spectra for level flight, illustrating repeatability between 2003 and 2004 test campaigns. The blue contour indicates the TR integration region.

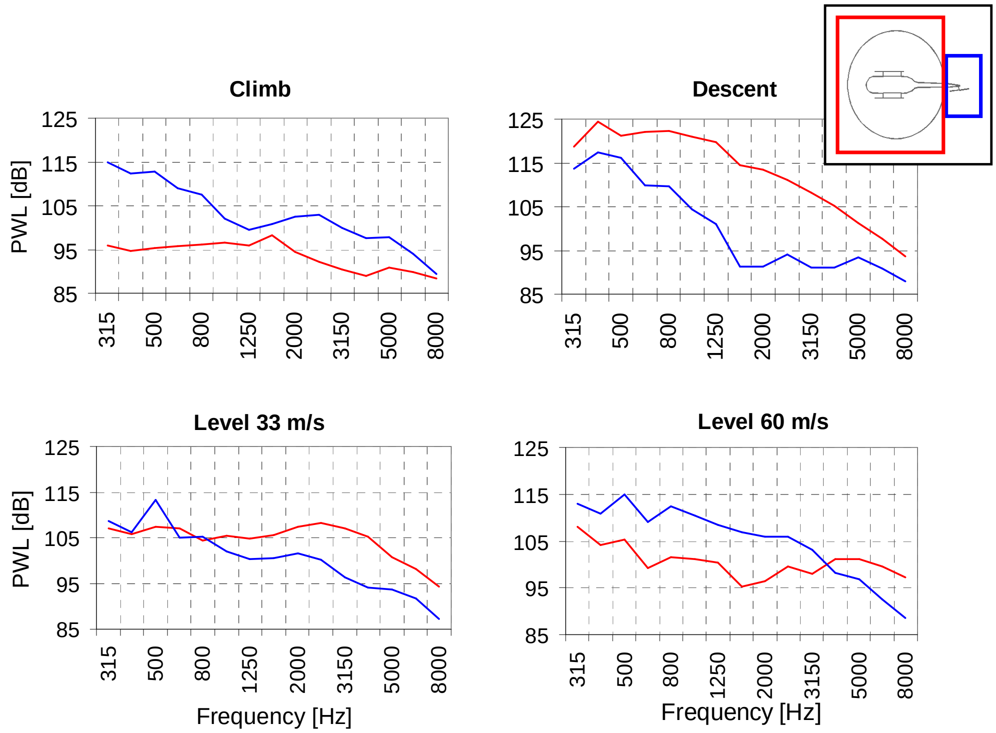

Fig. 7: Integrated MR (—) and TR (—) noise spectra for different flight conditions.

Source ranking

The relative importance of main- and tail rotor noise was determined by applying the power integration method to both regions (Fig. 7). The trends for the NACA0012 TR were the same as for the S102 TR shown here. It can be seen that for the climb condition the TR is dominant over the whole frequency range, while for descent flight the MR is always dominant (BVI noise). These results are consistent with the source plots in Fig. 5. For level flight the relative importance of main- and tail rotor depends on frequency and wind (flight) speed: the TR is most important at low frequencies and high wind speeds. Note that the lower spectra in Fig. 7 (e.g. the TR spectrum for the descent case) should be regarded as an upper limit for the real noise level, due to the possible influence of background noise on the integrated spectrum.

Interaction effects

The influence of the main rotor on tail rotor noise can be assessed by comparing integrated tail rotor noise spectra for the 'TR only' and 'MR+TR' configuration. Fig. 8 shows this comparison for the climb and high-speed level flight cases, since for these conditions TR noise is most important (see previous paragraph). The trends for the NACA0012 TR were the same as for the S102 TR shown here. Interestingly, the presence of the MR causes a small reduction in TR noise for the climb condition. For high-speed level flight, a small noise increase is observed at the higher frequencies. More information on MR-TR interaction was obtained from the ROSI results (page 9) and the inflow footprints (Section 3.2).

Reduction concepts

Using the power integration method, the effect of the different tail rotor noise reduction concepts was assessed as a function of frequency (Fig. 9). Again the tail rotor integration contour was used. It can be seen that reversal of tail rotor sense of rotation (from 'advancing side down' to 'advancing side up') gives a significant broadband noise reduction for both flight conditions. Note that the TR thrust was the same for both senses of rotation[2]. The other reduction concepts show generally smaller effects than the reversal of tail rotor sense of rotation, except the large reduction at 500 Hz due the reduced tip speed.

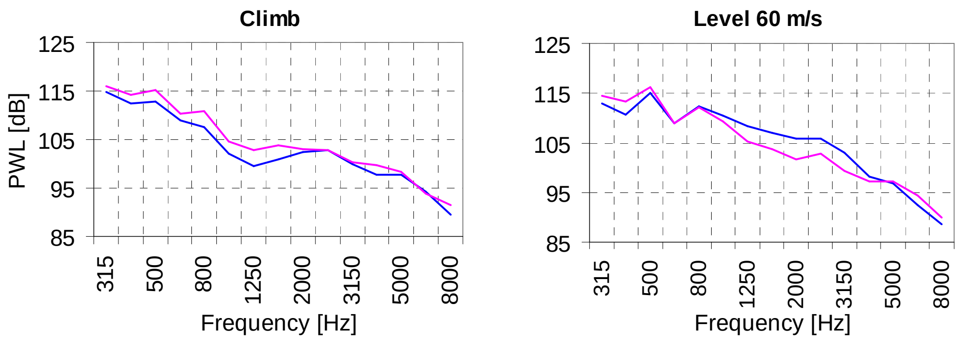

Fig. 8: Integrated TR noise spectra for 'TR only' (—) and 'MR+TR' (—) configuration.

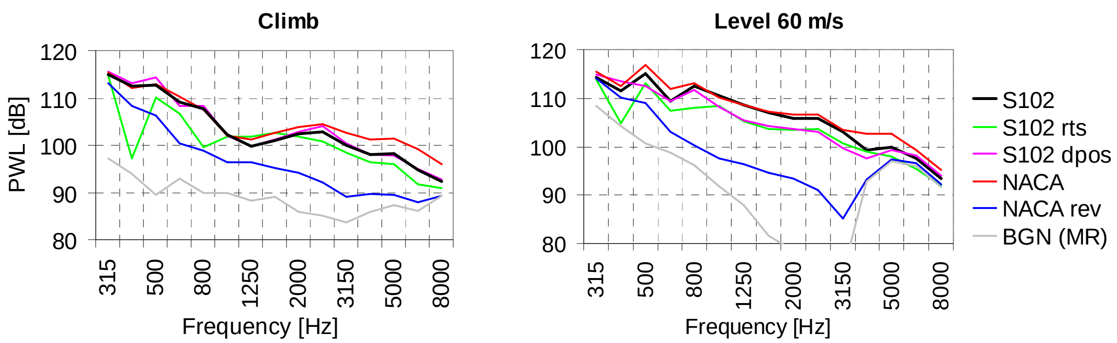

Fig. 9: Integrated TR noise spectra for different TR concepts: rts=reduced tip speed; dpos=change in TR position; rev=reversed sense of rotation; BGN=background noise ('MR only' case).

ROtating Source Identifier

In order to compare the noise sources for the different main rotor blades, a second processing method was applied to the array results (ROSI- Rotating Source Identifier[9]). Fig. 10 shows ROSI plots for the descent configuration together with the corresponding standard source plots, in which BVI noise is recognised. The ROSI plots show the source locations on the individual blades, averaged over 30 revolutions. Since these plots show the integrated noise production over all azimuthal angles, the orientation of the plot is arbitrary. It can be seen that there are only small differences in the BVI noise production of the different blades. Although ROSI was previously mainly used to identify broadband self-noise from rotor blades[5,6,9], these results illustrate that ROSI can also be applied to impulsive noise.

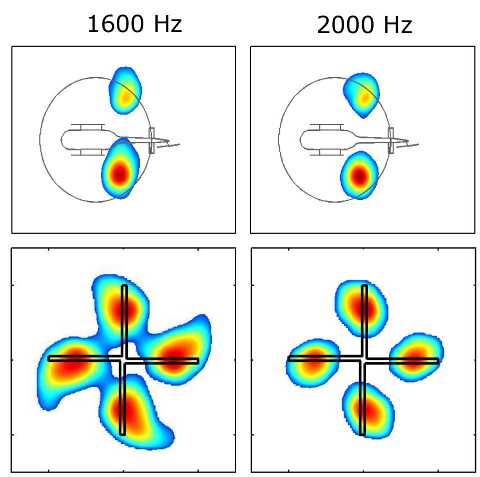

Fig. 10: Standard acoustic source plots (upper row) and corresponding ROSI plots (lower row) for the descent condition.

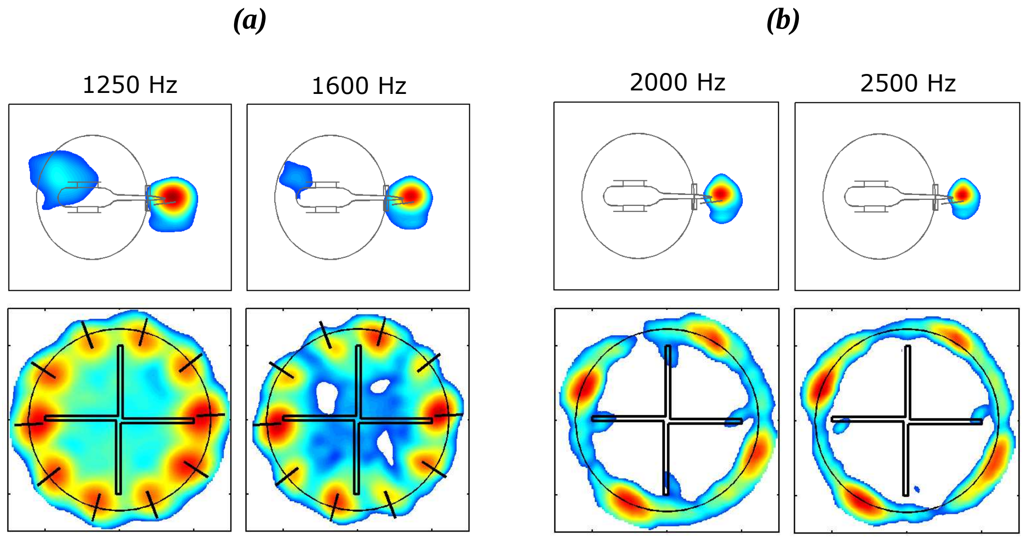

Fig. 11: Standard source plots (upper row) and corresponding ROSI plots (lower row) for high-speed level flight (a) and climb (b).

Besides the descent case, where the MR is dominant, ROSI was also applied to cases where the tail rotor noise was dominant. Again the scan plane was placed in the MR plane and rotated along with the MR blades. Surprisingly, this yielded interesting information on the dependence of tail rotor noise on main rotor azimuth. Fig. 11 shows standard source plots and ROSI plots for the level flight and climb condition. For the level flight condition, the phase difference between the main and (S102) tail rotor was nearly constant during the first 30 main rotor revolutions (only the first 30 main rotor revolutions were used for the ROSI plots). For the climb condition the phase difference was varying. The black circle in the ROSI plots indicates the position of the tail rotor center during the revolution of the main rotor. Since for the level flight condition the main and tail rotor were in phase, the tail rotor azimuth was directly coupled to the main rotor azimuth. Therefore, in Fig. 11*a* the positions where the tail rotor blades are horizontal can be indicated by the radial line segments (the length of the segments corresponds to the tail rotor diameter). Since the tail rotor RPM was five times higher than the main rotor RPM, and the tail rotor has two blades, there are 10 blade passages during one main rotor revolution.

The ROSI plots in Fig. 11*a* clearly show 10 sources, corresponding to the 10 tail rotor blade passages. Since the source radii are larger than the radius of the main rotor, the sources must be due to the tail rotor. The fact that the azimuthal source locations coincide with the line segments, shows that the tail rotor noise is produced when the blades are horizontal. Moreover, the source maxima are inside the tail rotor circle, indicating that the noise is produced by the upstream tail rotor blade. Interestingly, it can be seen that the two loudest blade passages are those where the tail rotor blade is closest to the main rotor blade. At 1.6 kHz, increased levels are also observed for the tail rotor passages directly after the passage of the other two main rotor blades. Thus, the ROSI plots clearly demonstrate the interaction between the main and tail rotor for the level flight condition, which is consistent with the noise increase at these frequencies in Fig. 8.

Fig. 11*b* shows example ROSI plots for the climb condition (NACA0012 TR). Since the phase difference between main and tail rotor was varying, there was no fixed relationship between the tail and main rotor azimuth. As a result, Fig. 11*b* does not show 10 sources, but a circular noise pattern. However, it can be clearly seen that on the average the tail rotor blades produce most noise just after the passage of the main rotor blades. Thus, the ROSI plots also demonstrate an interaction effect for the climb condition. However, the presence of an interaction effect does not necessarily result in a noise *increase*. As shown in Fig. 8, the presence of the main rotor did not give an increase in (S102) TR noise for the climb condition at 2 and 2.5 kHz. For the NACA0012 TR (not shown) even a small reduction was found at these frequencies. Apparently, the presence of the MR reduces the average TR noise level, even though Fig. 11*b* does show that local maxima occur after the passage of the MR blades.

3.2 Comparison to inflow footprints

In this section the array results are compared to the inflow footprints, to check the consistency between the two different methods. As illustrated in Fig. 4, both methods provide complementary information on the location and directivity of the noise sources: whereas the inflow footprints show the *overall* noise radiation (from all sources) in *different* directions, the phased array identifies the *different* sources for a *fixed* observer position (i.e. the array position). It should be noted that for a good comparison between the array results and the inflow footprints, only the part of the footprint in the direction of the out-of-flow array should be regarded. Therefore, in this section the projection of the array on the inflow scan plane will be indicated in the footprints. The position of this projection depends on array position and source location (Fig. 12). In this section first the familiar case of MR noise for the descent condition will be discussed, to introduce the relation between array results and inflow footprints. Subsequently it is checked whether the array observations regarding TR noise reduction concepts, source ranking, and interaction effects are reproduced in the inflow footprints. The inflow footprints are presented in 1/3-octave bands to allow good comparison to the source plots.

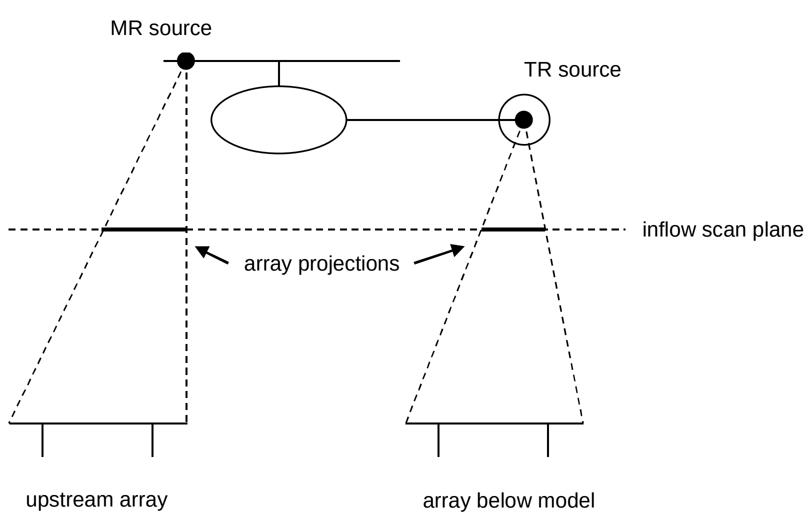

Fig. 12: Projection of array surface on inflow scan plane.

MR noise for descent condition

Fig. 13 shows acoustic source plots for both array positions in the descent case. As a reference the pressure history for a transducer on the outer blade is shown as well (zero azimuth is when the blade points downstream). The source plots clearly show that MR noise is dominant over

TR noise. Furthermore, for the upstream array position the advancing side is dominant, while for the array position below the model the retreating side is dominant. The azimuth angles for the dominant source positions are about 60° and 310°, which is consistent with the BVI positions in the blade pressure history. The range of the color scale for the source plots is 12 dB, but it should be noted that the maximum in the upstream source plot is 8 dB higher than the maximum for the 'below model' plot. Since the source levels are normalised to a constant distance, this means that the advancing side source is 8 dB louder than the source on the retreating side (for the present radiation directions).

More insight in the radiation characteristics of the BVI noise can be obtained by comparing the source plots to the inflow footprint at the same frequency (Fig. 14). The range of the color scale is again 12 dB. In order to allow a good comparison, the projection of the phased array surface on the inflow scan plane (as 'seen' from the dominant source locations in Fig. 13) is plotted for both array positions (see also Fig. 12). By comparison with Fig. 13, it can be seen that the major red spot in Fig. 14 is due to the advancing side source, whereas the green source area more downstream is due to the source on the retreating side. The level difference between these two source regions is consistent with the difference between the maxima in the source plots of 8 dB. Thus, the array provides additional information about the source locations and directivity that cannot be extracted from the inflow footprints alone.

TR noise reduction concepts

The array results indicated a large reduction in TR noise due to a reversal of TR sense of rotation (Fig. 9). As an example, the corresponding inflow footprints at 1.6 and 2 kHz for the climb condition are shown in Fig. 15. The projection of the (downstream) array surface on the inflow scan plane, as 'seen' from the TR position, is again indicated in the footprints. This illustrates that the noise received by the array constitutes only a small

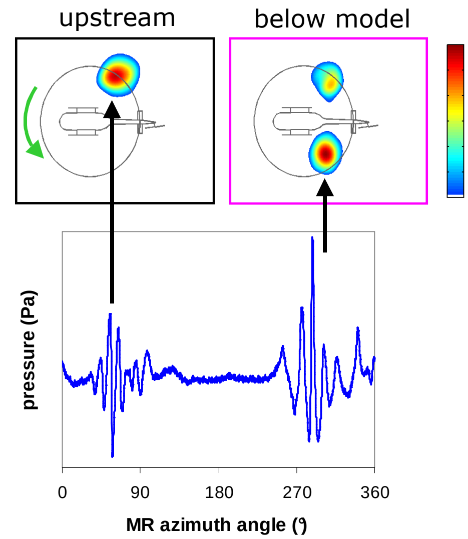

Fig. 13: Acoustic source plots (2 kHz) and blade pressures showing BVI noise for the descent condition.

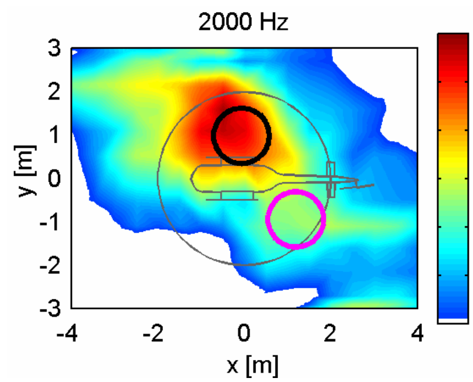

Fig. 14: Inflow footprint for the descent condition. The projection of the phased array surface on the inflow plane is indicated by circles (for both array positions).

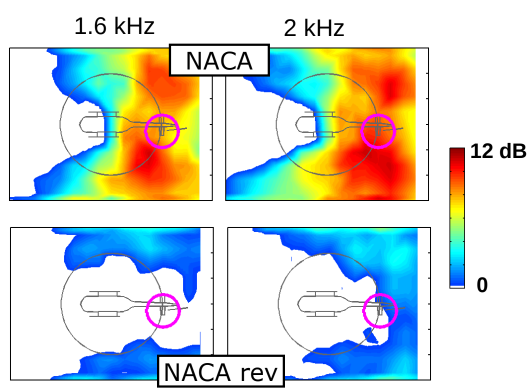

Fig. 15: Inflow footprints for the climb condition, with normal and reversed TR sense of rotation.

part of the total radiation pattern, which should be realised when interpreting the array results. Similar to the integrated array spectra, the footprints also exhibit a significant noise reduction for the reversed sense of rotation. This qualitative correspondence between array results and inflow footprints was generally also found for the other frequencies, for other TR noise reduction concepts, and for the high-speed level flight condition.

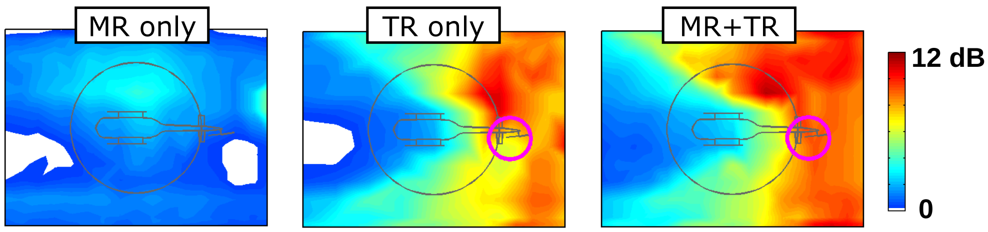

Fig. 16: Inflow footprints (1.6 kHz) for the high-speed level flight condition (S102 TR).

Source ranking and interaction effects

The array results indicated that TR noise is most important in the climb and high-speed level flight conditions (Fig. 7). These trends were also found in the inflow footprints. As an example, Fig. 16 shows the inflow footprints at 1.6 kHz for the high-speed (60 m/s) level flight condition. By comparing the 'MR only' and the 'TR only' plots, it can be seen that, in agreement with the array results, the TR is clearly dominant. Thus, with regard to the relative importance of MR and TR noise, the inflow footprints were generally consistent with the array results for all conditions.

Next, it was checked if the array conclusions with regard to interaction effects were also reproduced in the inflow footprints. By comparing the 'TR only' and 'MR+TR' plots in Fig. 16, it can be seen that due to the presence of the MR a small increase in TR noise occurs, which is consistent with the array results for the high-speed level flight condition (Fig. 8). However, for the interaction effect in the *climb* condition a discrepancy was found between the array results and the inflow footprints. This is shown in Fig. 17 and Fig. 18 for the NACA0012 TR. Whereas the integrated TR noise spectra and the acoustic source plots indicate a TR noise *decrease* due to the presence of the MR (similar to the S102 TR in Fig. 8), the inflow footprints show an *increase* in noise at the same frequency. In the 'MR+TR' plot in Fig. 18 the inflow measurement grid is plotted, indicating that there are only three measurements points in the array projection.

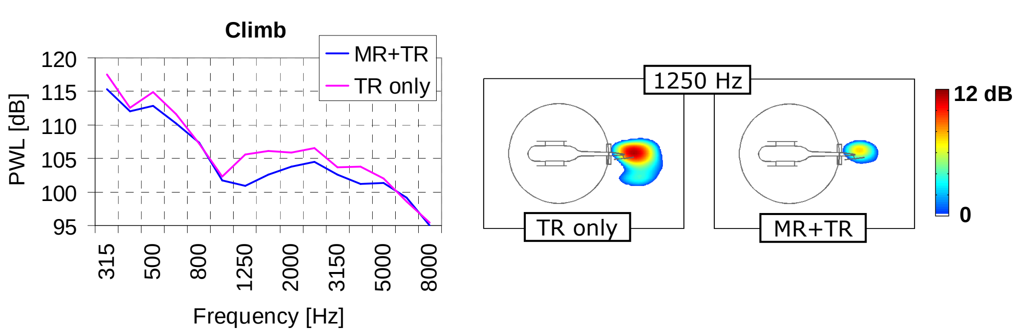

Fig. 17: Integrated TR noise spectra and source plots for the climb condition (NACA0012 TR).

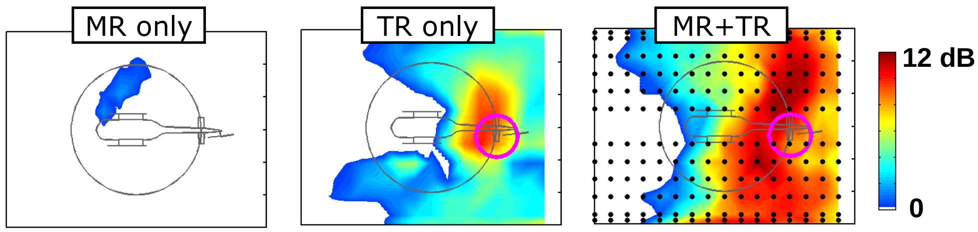

Fig. 18: Inflow footprints (1250 Hz) for the climb condition (NACA0012 TR).

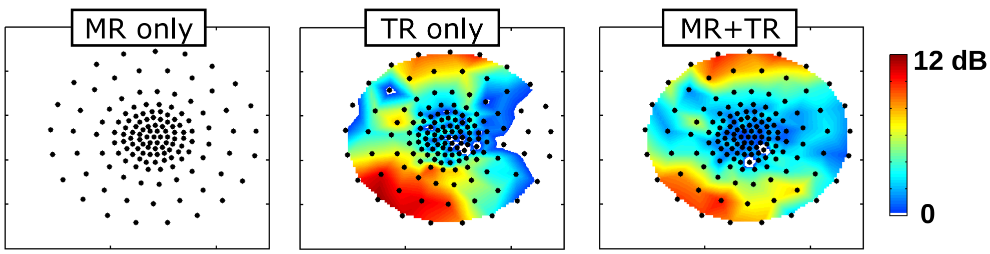

Fig. 19: Array footprints (1250 Hz) for the climb condition (NACA0012 TR).

To further investigate this discrepancy between the array results and the inflow footprints, Fig. 19 shows the sound levels measured on the out-of-flow array microphones. The microphone positions are indicated by the black dots. These plots only show a small difference between the 'TR only' and 'MR+TR' case, suggesting a small interaction effect. In summary, at 1250 Hz the inflow footprints show a noise increase, the integrated array spectra show a significant decrease, and the measured levels on the array microphones suggest a small effect.

In Fig. 20 the interaction effect (i.e. the increase in TR noise due to the presence of the MR) is quantified as a function of frequency for the three different methods: the integrated array spectra ('powint'), the inflow footprints ('inflow'), and the average measured spectra on the array microphones ('arraymics'). For the inflow footprints the average of the three microphones within the array projection (see Fig. 18) was used. It can be seen that the measured array spectra follow the integrated array spectra quite well at low and high frequencies. This is expected, because the TR is the dominant noise source for the climb condition (see Fig. 7). However, for the intermediate frequencies a difference occurs, for

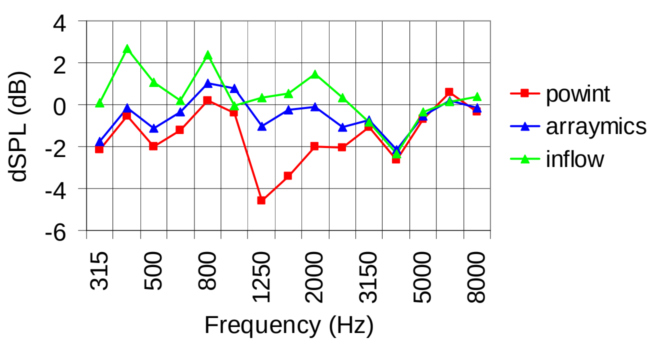

Fig. 20: Interaction effect for the climb condition, for three different methods.

which no conclusive explanation is available. A possible explanation for the lower integrated TR noise levels in the presence of the MR could be that the TR noise propagates through the MR downwash, which may cause coherence loss. However, if this is the case it would also be expected at higher frequencies.

For the high frequencies, the inflow footprints nicely coincide with the array results. However, for intermediate and low frequencies, the values for the inflow footprints are generally higher than for the array. A possible reason for this discrepancy may be the relatively low density of the inflow measurement grid (compared to the spatial density of the array microphones), as a result of which the inflow footprint may 'miss' some directional effects. Another possible reason may be that the inflow footprint is measured in the geometric nearfield of the model, whereas the array measurements are done in the farfield. Finally, the array measurements may suffer from shielding effects, due to the structures between the array and the model.

4 CONCLUSIONS

The out-of-flow array results in the present report have illustrated the capabilities of the acoustic array technique for helicopter rotor noise. Main- and tail rotor noise sources were characterized as a function of frequency for various flight conditions. The analysis showed that TR noise is dominant for climb and high-speed level flight. By comparing TR noise spectra for the 'TR only' and 'MR+TR' cases, small interaction effects could be shown. Furthermore, several TR noise reduction concepts were assessed, which showed that, besides a reduction of rotor tip speed, reversal of TR sense of rotation is most significant.

Using a processing method for rotating sources, small noise differences between individual MR blades could be identified. Surprisingly, this method also clearly showed the dependence of TR noise on the azimuthal position of the MR blades for the cases where TR noise is dominant.

The array results were also compared with the more conventional inflow footprints, to check the consistency between the two different methods. It was shown that the array provides additional information on source locations and directivity, which cannot be extracted from the inflow footprints. Therefore, it is best to measure both inflow footprints and phased array source maps. The array results generally show the same trends as the inflow footprints for the noise reduction concepts, for the relative importance of MR and TR noise, and for MR-TR interaction effects. Only for the interaction effect in the climb condition some discrepancies are found, for which no conclusive explanation is available yet. Possible explanations include coherence loss due to MR downwash, the relatively low density of the inflow measurement grid, nearfield/farfield effects, or shielding effects.

5 REFERENCES

[1] Langer, H.J., Dieterich, O., Oerlemans, S., Schneider, O., Van der Wall, B., Yin, J., "The EU HeliNOVI project- wind tunnel investigations for noise and vibration reduction", Proceedings of the 31st European Rotorcraft Forum, Florence, Italy (September 2005).

[2] Yin, J., Van der Wall, B., Oerlemans, S., "Representative test results from HeliNOVI aeroacoustic main rotor/tail rotor/fuselage test in DNW", Proceedings of the 31st European Rotorcraft Forum, Florence, Italy (September 2005).

[3] Oerlemans, S., and Sijtsma, P., "Acoustic Array Measurements of a 1:10.6 Scaled Airbus A340 Model", AIAA paper 2004-2924 (2004).

[4] Sijtsma, P., and Stoker, R.W., "Determination of Absolute Contributions of Aircraft Noise Components using Fly-Over Array Measurements", AIAA paper 2004-2958 (2004).

[5] Oerlemans, S., Schepers, J.G., Guidati, G., and Wagner, S., "Experimental Demonstration of Wind Turbine Noise Reduction through Optimized Airfoil Shape and Trailing-Edge Serrations", presented at the European Wind Energy Conference, Copenhagen (2001).

[6] Oerlemans, S. and Méndez López, B., "Acoustic Array Measurements on a Full Scale Wind Turbine", AIAA paper 2005-2963 (2005).

[7] Oerlemans, S., and Migliore, P., "Aeroacoustic wind tunnel tests of wind turbine airfoils", AIAA paper 2004-3042 (2004).

[8] Brooks, T.F., Marcolini, M.A., and Pope, D.S., "A directional array approach for the measurement of rotor noise source distributions with controlled spatial resolution", Journal of Sound and Vibration 112 (1987).

[9] Sijtsma, P., Oerlemans, S., and Holthusen, H., "Location of rotating sources by phased array measurements", AIAA paper 2001-2167 (2001).

[10] Blacodon, D., Elias, G., Prieur, J., and Papillier, D., "Noise source localization on a Dauphin helicopter in flight", Journal of the American Helicopter Society Vol. 49, no. 4 (2004).

[11] Holthusen, H., and Smit, H., "A new data-acquisition system for microphone array measurements in wind tunnels", AIAA paper 2001-2169 (2001).

[12] Johnson, D.H., and Dudgeon, D.E., "Array Signal Processing", Prentice Hall (1993).

[13] Amiet, R.K., "Refraction of Sound by a Shear Layer", Journal of Sound and Vibration, Vol. 58, No. 2, pp. 467-482, 1978.